Received: 30 August 2022 | Revised: 31 October 2022 | Accepted: 6 November 2022

DOI: 10.1002/pro.4504

FULL-LENGTH PAPER

THE PROTEIN SOCIETY WILEY

Higher-order interactions of Bcr-Abl can broaden chronic myeloid leukemia (CML) drug repertoire

Yonglan Liu[1] | **Mingzhen Zhang**[2] | **Hyunbum Jang**[2] | **Ruth Nussinov**[2,3]

[1]Cancer Innovation Laboratory, National Cancer Institute, Frederick, Maryland, USA

[2]Computational Structural Biology Section, Frederick National Laboratory for Cancer Research, Frederick, Maryland, USA

[3]Department of Human Molecular Genetics and Biochemistry, Sackler School of Medicine, Tel Aviv University, Tel Aviv, Israel

Correspondence
Ruth Nussinov, Computatoinal Structural Biology Section, Frederick National Laboratory for Cancer Research, Frederick, MD 21702, USA.
Email: nussinor@mail.nih.gov

Funding information
National Cancer Institute, Grant/Award Number: HHSN261201500003I; National Institutes of Health (NIH); CCR

Review Editor: John Kuriyan

Abstract

Bcr-Abl, a nonreceptor tyrosine kinase, is associated with leukemias, especially chronic myeloid leukemia (CML). Deletion of Abl's N-terminal region, to which myristoyl is linked, renders the Bcr-Abl fusion oncoprotein constitutively active. The substitution of Abl's N-terminal region by Bcr enables Bcr-Abl oligomerization. Oligomerization is critical: it promotes clustering on the membrane, which is essential for potent MAPK signaling and cell proliferation. Here we decipher the Bcr-Abl specific, step-by-step oligomerization process, identify a specific packing surface, determine exactly how the process is structured and identify its key elements. Bcr's coiled coil (CC) domain at the N-terminal controls Bcr-Abl oligomerization. Crystallography validated oligomerization via Bcr-Abl dimerization between two Bcr CC domains, with tetramerization via tight packing between two binary assemblies. However, the structural principles guiding Bcr CC domain oligomerization are unknown, hindering mechanistic understanding and drugs exploiting it. Using molecular dynamics (MD) simulations, we determine that the binary complex of the Bcr CC domain serves as a basic unit in the quaternary complex providing a specific surface for dimer–dimer packing and higher-order oligomerization. We discover that the small α1-helix is the key. In the binary assembly, the helix forms interchain aromatic dimeric packing, and in the quaternary assembly, it contributes to the specific dimer–dimer packing. Our mechanism is supported by the experimental literature. It offers the key elements controlling this process which can expand the drug discovery strategy, including by Bcr CC-derived peptides, and candidate residues for small covalent drugs, toward quenching oligomerization, supplementing competitive and allosteric tyrosine kinase inhibitors.

KEYWORDS

Bcr, covalent inhibitors, fusion protein, molecular dynamics, oligomerization domain, peptide inhibitor

1 | INTRODUCTION

Oncogenesis initiating with the reciprocal translocation of Chromosome 22 containing a breakpoint cluster region (*BCR*) gene and Chromosome 9 containing the Abelson (*ABL*) protooncogene is the driver of leukemia (Lindström & Friedman, 2020; Manley et al., 2020; Quach et al., 2021). The fusion between the *BCR* gene and the upstream of the *ABL* gene yields the *BCR-ABL* fusion gene that encodes an oncogenic protein, Bcr-Abl. Bcr-Abl exhibits constitutive tyrosine kinase activity, leading to abnormal cell signal transduction and blastic transformation (Alves et al., 2021; Modi et al., 2011; Mughal et al., 2016; Reckel et al., 2017). Depending on the exact breakpoints in the translocation, different isoforms of Bcr-Abl can be produced, including the p190, p210, and p230 forms that are associated with B-cell acute lymphoblastic leukemias, chronic myeloid leukemia (CML), and neutrophilic-CML (CML-N), respectively (Ren, 2005). The requirement of the N-terminal oligomerization region of Bcr-Abl for kinase activation, which is analogous to the biological function of oligomerization of receptor tyrosine kinases (Peiris et al., 2020; Schlessinger, 2000), has been implicated in a wide range of studies (He et al., 2002; Mian et al., 2009; Ross & Mgbemena, 2014; Zhang et al., 2001). This so-called coiled coil (CC) region was first proposed by Crick in 1953. Except for the *ABL1* gene, the *BCR* gene was identified to cement other genes, such as Janus kinase 2, platelet-derived growth factor receptor alpha, ret proto-oncogene, and fibroblast growth factor receptor1 (*FGFR1*), to generate different fusion proteins (Peiris et al., 2020). In particular, *BCR-FGFR1* fusion occurring in stem cell leukemia/lymphoma drives the progression of atypical CML, acute myeloid leukemia, and B-cell lymphoma. Oligomerization of the Bcr region mediates Bcr-FGFR1 activation (Peiris et al., 2020).

The Bcr CC domain is a region preferring to form an α-helical tetramer (Smith et al., 2003; Zhao et al., 2002). Tetramerization of the CC domain in the Bcr region increases the concentration of Bcr-Abl at the membrane, which has been shown to be especially important for its tyrosine kinase activity (Zhang et al., 2001). Biological and biophysical data have shown that Bcr-Abl oligomerization promotes its trans-autophosphorylation (Dixon et al., 2011). Bcr-Abl with deletion of the CC domain (Residues 1–63) displays a diminished autophosphorylation capability comparing to its wild-type form (He et al., 2002). Inhibition of CC oligomerization largely reverses the tyrosine kinase activity of Bcr-Abl, thus abrogating transformation and leukemogenesis (Smith et al., 2003). Mutations with ablation or alanine substitution of the N-terminal CC domain of p210 Bcr-Abl impaired oligomerization, resulting in dysregulation of its in vivo kinase activity (Smith et al., 2003). Consequently, transformation of primary bone marrow B-lymphoid was abolished. Additionally, the Bcr-Abl CC domain governs its subcellular localization in the cytoplasm, which is crucial for the development of CML (Peng et al., 2021).

The emergence of imatinib, an orthosteric tyrosine kinase inhibitor (TKI) occupying the APT-binding pocket in the inactive state of the Abl kinase domain, and weakening its phosphorylation ability (Astl & Verkhivker, 2019; Lindström & Friedman, 2022; Liu, Zhang, et al., 2022; Verkhivker, 2021; Yeung et al., 2021), has proven a revolutionary advance in the therapy of Bcr-Abl-associated leukemia. Most patients who were administered imatinib have had a lifespan indistinguishable from healthy people (Kantarjian & Cortes, 2014). Orthosteric TKIs, such as bosutinib, dasatinib, nilotinib, ponatinib, and bosutinib (Chen et al., 2017; Nussinov et al., 2022; Shah & Sawyers, 2003) as well as the new allosteric TKI, asciminib (Eide et al., 2019; Hughes et al., 2019; Schoepfer et al., 2018; Wylie et al., 2017), differ in their inhibitory efficacies against Bcr-Abl. Additional therapeutic strategies are expected to arise as either the main vehicle, or as adjuvant therapy, or increasingly, combinatorial regimes. The Bcr-Abl CC domain can be a drug target as an alternative to the kinase domain of Abl that is inhibited by occupancy-based or allosteric TKIs, or in combination. Peptides have been designed to prevent Bcr-Abl oligomerization. They were delivered into leukemic cells and inhibited cell proliferation. Peptides extracted from the Bcr CC region can interfere with Bcr-Abl oligomerization, weaken the catalytic activity and the transformation potential of Bcr-Abl and its mutants, and even increase their kinase sensitivity to imatinib (Beissert et al., 2003, 2008). By substituting specific residues of the Bcr CC domain, mutant peptides exhibit higher affinity toward the CC region of Bcr-Abl over itself, leading to their preferential specificity for hetero-oligomer with Bcr-Abl (Bruno & Lim, 2015; Dixon et al., 2012; Woessner et al., 2015). These mutant peptides have been shown to potently inhibit Bcr-Abl kinase activity both in vivo and in vitro by preventing Bcr-Abl homo-oligomerization. Importantly, once delivered into leukemic cells, mutant CC peptides can reduce the colony ability, inhibit the transformative activity, and induce apoptotic possibility of cells that express wild-type Bcr-Abl or TKIs-resistant Bcr-Abl mutants. These impressive results underscore disrupting Bcr-Abl oligomerization as a promising therapeutic strategy for suppressing Bcr-Abl oncogenicity. They highlight the importance of the underlying detailed structural mechanism of oligomerization of the Bcr CC domain as possible alternative therapy against Bcr-Abl-induced leukemia beyond TKIs.

The overall structure of the Bcr CC domain has been captured by x-ray crystallography (Zhao et al., 2002), showing that it preferentially adopts a quaternary complex with two binary assemblies cross-packing each other. The interface of the binary assembly was also identified. Each binary assembly packs in a "knobs-into-holes" mode, common in the CC domains of other proteins, such as epidermal growth factor receptor (Mozumdar et al., 2020), fibrinogen (Kollman et al., 2009), geminin superfamily (Caillat et al., 2015), vimentin (Chernyatina et al., 2012), GCN4 (Utterstrom et al., 2021), activator protein-1 (Yin et al., 2017). Subsequently, several studies designed Bcr CC-derived peptide inhibitors that outcompete the CC domains interaction (Beissert et al., 2003, 2008; Bruno & Lim, 2015; Dixon et al., 2011, 2012). However, there is an additional region, the α1-helix, which is involved in both the monomer–monomer packing for binary assembly and the dimer–dimer packing for quaternary assembly, and its function has been unclear. Further, the quaternary form of the Bcr CC domain shows remarkable differences from that of other CC domains, and exactly what leads to the specific packing of the Bcr CC tetramer is still elusive. Questions as to why the Bcr CC domain favors the quaternary complex in the form of dimer–dimer packing and why its higher-order oligomeric assemblies cannot be formed, are also still unanswered. In this work, using molecular dynamics (MD) simulations, we seek to address these questions, as well as detail the underlying mechanism of oligomerization of the Bcr CC domain. Collective data showed that the populated oligomerization (or tetramerization) pathway of the Bcr CC domain is a stepwise process. Understanding this process and factors controlling it is important for mechanistic insight and may help effective inhibitor design. The binary assembly serves as the building block of the tetramer. Upon dimerization, the binary Bcr CC generates two surfaces: Surface 1 is responsible for the dimer–dimer interaction to form the quaternary complex and Surface 2 is exposed to solvent. Steric hinderance and unbalanced charge of Surface 2 that are induced by the linker connecting helix α1 and α2, disfavor its interacting ability. Herein, higher-order oligomers of the Bcr CC domain are unlikely to be formed. The α1-helix conducts different functions for the binary and quaternary complexes. It interacts with the α2-helix through interchain aromatic interaction, assisting the monomer–monomer packing for the binary form. Importantly, we emphasize that helix α1 is required for specific packing between the two binary Bcr CCs in the quaternary complex. Deletion of the entire helix leads to destabilization of this specific packing. In addition, salt bridges mediate both the monomer–monomer and dimer–dimer interactions. Altogether, we determined key parameters that control dimerization and tetramerization of the Bcr CC domain and detailed the stepwise oligomerization process, which can be exploited to pharmaceutically forestall Bcr-Abl homo-oligomerization or clustering. The identification of candidate residues on the relevant surfaces raises the feasibility of covalent molecular inhibitors that hamper the binary and quaternary packing or interfere with its precise organization.

2 | RESULTS

2.1 | Characterization of binary and quaternary Bcr CCs

The Bcr CC domain has 72 amino acids (Figure 1a), consisting of two parallel helices, a short α1-helix (Residues 5–15) and a long α2-helix (Residues 28–67), connected by a short linker. The parallel alignment of the helices yields an N-shaped structure. In the binary assembly, two α2-helices align to form an antiparallel CC, where α2-helix is sandwiched by partner's α1-helices and α2-helices (Figure S1). The α2–α2 packing displays a canonical "knobs-into-holes" mode, which is underpinned by the seven-residue heptad repeats, $(abcdefg)_n$ (Figure 1b; Ludwiczak et al., 2019; Lupas et al., 2017). Residues at the core-forming positions of *a* and *d* are predominantly hydrophobic. At the α2–α2 interface, residues at the *a*(*d*) positions from one helix (knob) geometrically match the cavities formed by the sidechains of the partner helix (hole), which dominates the CC folding. However, E52 at the *d* position of a heptad repeat is an exception for the α2-helix of the Bcr CC domain. This negatively charged residue preferentially forms an intrachain salt bridge with R55 at the *g* position. In the binary complex, the α1–α2 interaction mainly results from the aromatic interactions between F7/W11 in the α1-helix of one monomer and F54/Y58 in the α2-helix of the neighboring monomer. The α1–α2 interaction was identified as assisting the packing stability of the CC (Zhao et al., 2002). The quaternary complex of Bcr CC domain presents a unique dimer–dimer packing with a crossing angle of ∼130° between the CC axes of one dimeric unit (dimer 1) to the other (dimer 2; Figure S1; Zhao et al., 2002). R43/N50 at the *b* position and E46/R53 at the *e* position in the four α2-helices form the salt bridges and hydrogen bonds in the middle region, which we term "dimer–dimer α2–α2 interaction". Additionally, the two α1 helices in one dimeric unit contact with the two edging regions of the other dimeric unit, for which A10/A13 in the α1-helix of one chain of one dimeric unit form the hydrophobic interactions with A64 in the α2-helix of one chain of the other dimeric unit. Here, we term it as

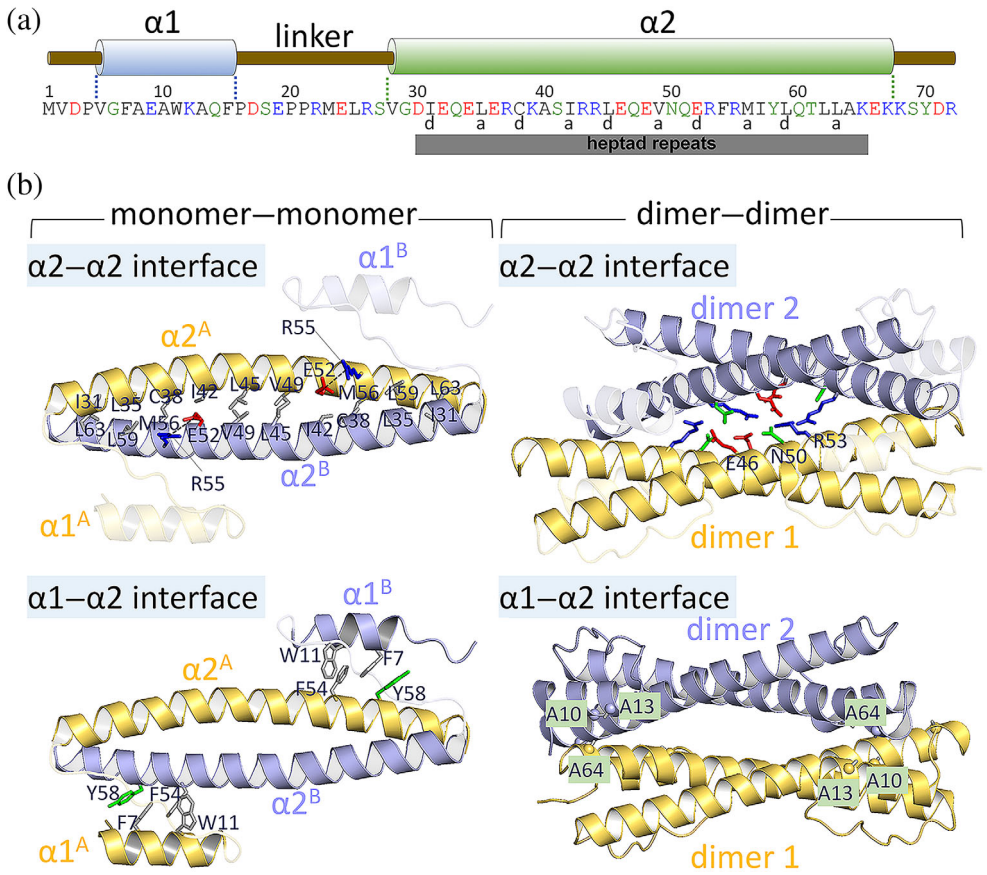

FIGURE 1 Sequence, structure, and interface. (a) Sequence and components, and (b) structures and interfaces for the binary and quaternary complexes, of the Bcr CC domain. The binary complex contains chains A and B (yellow and lightblue), and the quaternary complex contains two dimeric units, dimer 1 (chain A/B, yellow) and dimer 2 (chain C/D, lightblue). Each chain in the binary Bcr CC consists of an α1-helix (e.g., $\alpha1^A$ for chain A and $\alpha1^B$ for chain B) and an α2-helix (e.g., $\alpha2^A$ for chain A and $\alpha2^B$ for chain B), which are connected by a linker. Interfacial residues are showed as sticks. The positively charged, negatively charged, polar, and hydrophobic residues at the interfaces are colored in blue, red, green, and gray, respectively

"dimer–dimer α1–α2 interaction". Four regions of such interaction exist in the quaternary complex.

2.2 | Bcr CC domain favors to form the binary and quaternary complex

The unveiled crystal structures delineate the oligomerization of the Bcr CC domain, in which the domains predominately aggregate as a binary or a quaternary complex. This leads us to speculate that a higher-order oligomer larger than the quaternary complex hardly occurs to the Bcr CC domain. To validate this speculation, we first constructed models of the ternary complex of the Bcr CC domain based on the crystal structure of the quaternary complex (Zhao et al., 2002). Alternative deletion of one chain in one of the dimeric units yields two models of the ternary complex, CC3m1 with chains A/B-C and CC3m2 with chains A/B-D (Table S1). Two microseconds simulations were performed for all systems. As expected, we observed that both binary and quaternary complexes, CC2m with chains A/B and CC4m with chains A/B–C/D are highly stable during the simulations (Figure 2a). CC2m conserves the monomer–monomer α1–α2 aromatic and α2–α2 hydrophobic interactions. In addition to the interactions at the dimeric interface, CC4m also preserves the dimer–dimer α1–α2 and α2–α2 interactions (Figure 2b). In sharp contrast, due to a lack of the counterpart chain, both ternary complexes, CC3m1 and CC3m2 exhibit remarkable conformational changes, displaying either the twisted α2-helix or disordered α1-helix (Figure 2a). We observed high fluctuations in the third chain compared with the corresponding chains in the CC4m system (Figure 2b). This is an apparent indicator that the binary complex is the basic building unit indispensable for Bcr CC tetramerization. To evaluate the binding affinities between chains A and B for the binary complex, between chains A/B and C (or A/B and D) for the ternary complex, and between chains A/B and C/D for the quaternary complex, we calculated the binding free energies for the four systems (CC2m, CC3m1, CC3m2, and CC4m) using molecular mechanics energies combined with the generalized Born surface area continuum solvation (MM-GBSA; Figure 2c). For CC2m, the favorable monomer–monomer packing resulted in the extremely low binding free energy of ~ -142.4 kcal/mol. For CC4m, the two dimeric units exhibited weaker packing than the monomer–monomer packing, showing ~40% increase of the binding free energy (~ -85.2 kcal/mol) comparing to the binary system. Although, within the simulation timescale, no disruption of the single chains (chain C or D) in the ternary

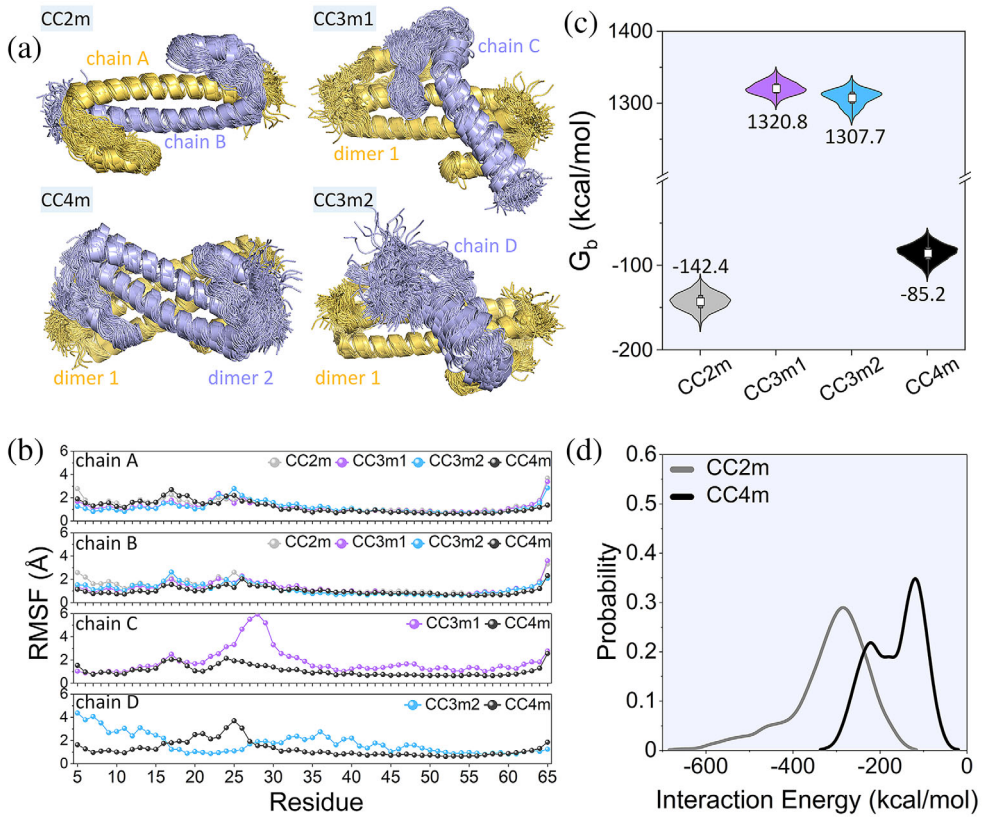

FIGURE 2 Bcr CC domain favors to form the binary and quaternary complexes. (a) Dynamics behaviors, (b) root mean square fluctuations (RMSFs) of each chain of the Bcr CC domain for the four systems of CC2m, CC3m1, CC3m2, and CC4m. (c) Binding free energy, $< G_b >$, between chain A and chain B for CC2m, dimer 1 and chain C (or D) for CC3m1 (or CC3m2), and dimer 1 and dimer 2 for CC4m. The average values are marked out. (d) Probability distributions of the monomer–monomer and dimer–dimer α2–α2 interaction energies for the CC2m and CC4m systems, respectively. The aligned structures in (a) and the data in (b), (c), and (d) were extracted from the last 1-μs trajectories. Chains A and B are colored in yellow and light blue for CC2m, respectively; dimer 1 and chain C (or D) for CC3m1 (or CC3m2) are colored in yellow and light blue, respectively; dimer 1 and dimer 2 for CC4m are colored in yellow and light blue, respectively

systems was observed, the single chain interactions with the dimeric unit are not favorable for the binding, which can be supported by the remarkably high binding free energies (∼1,320.8 kcal/mol for CC3m1 and ∼ 1,307.7 kcal/mol for CC3m2). This is mainly ascribed to the extremely high entropy caused by the conformational changes in the single chain of the ternary systems (Figure S2). Further, we calculated the interaction energies between the α2-helix of chain A and the α2-helix of chain B (monomer–monomer α2–α2 interaction) for CC2m, and between the two α2 helices in chains A/B and the two α2 helices in chains C/D (dimer–dimer α2–α2 interaction) for CC4m. For CC4m, two peaks are observed for the interaction energy between the two dimers. However, the second peak at ∼ − 110 kcal/mol is more significant than the first peak at ∼ − 240 kcal/mol. The peak at ∼ − 110 kcal/mol is used for comparison. The distribution profile of the monomer–monomer α2–α2 interaction energy peaked at ∼ − 300.0 kcal/mol for CC2m, much lower than the dimer–dimer α2–α2 interaction energy peak at ∼ − 110 kcal/mol for CC4m (Figure 2d). This suggests the "knobs-into-holes" packing between the two α2 helices in the binary complex is much stronger than hydrophilic interaction in the middle region of the α2 helices in the quaternary complex. Taken together, the Bcr CC domain is favorable for forming binary and quaternary complexes. The binary complex is the basic block for tetramerization.

2.3 | α1-helix assists monomer–monomer packing in dimeric Bcr CC

The α-helical CC with the "knobs-into-holes" packing mode (Figure 1b) is a ubiquitous motif in protein folding (Caillat et al., 2015; Chernyatina et al., 2012; Kollman et al., 2009; Ludwiczak et al., 2019; Mozumdar et al., 2020; Utterstrom et al., 2021; Yin et al., 2017),

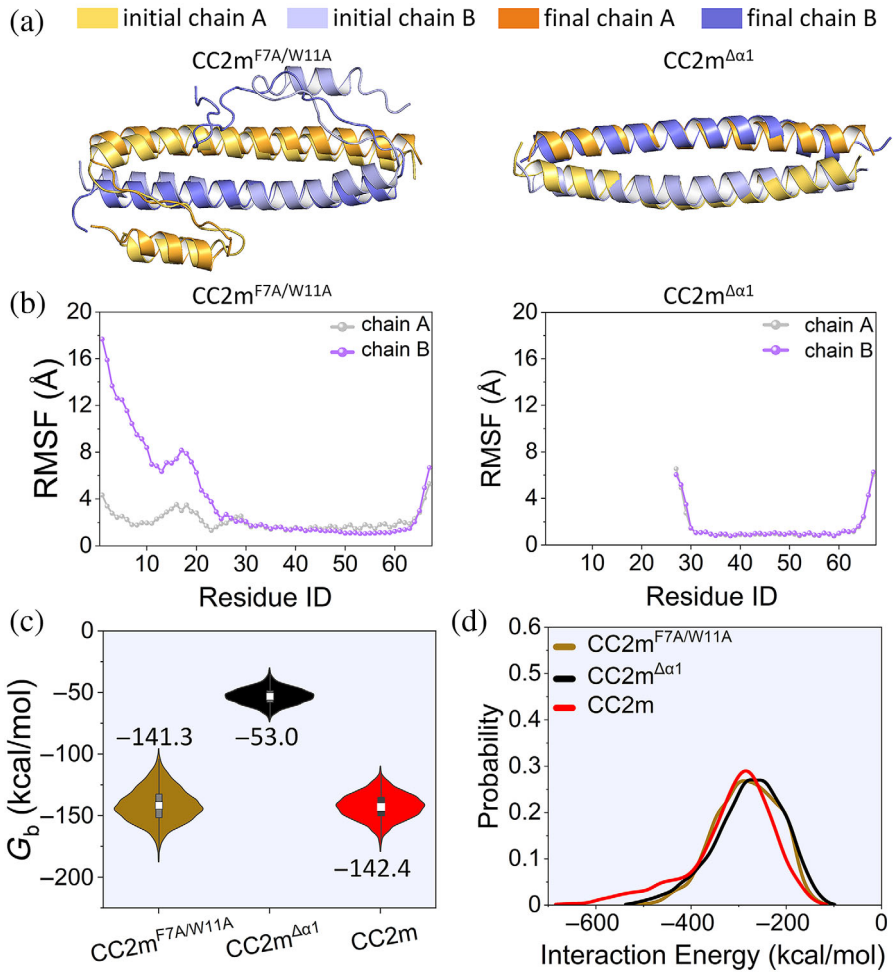

FIGURE 3 α1-helix assists monomer–monomer packing in the dimeric Bcr CC. (a) Structural alignment of the final to initial configurations, (b) RMSFs of chains A and B, (c) binding free energy, $< G_b >$, between chains A and B, and (d) probability functions of the monomer–monomer α2–α2 interaction energies for the three systems of $CC2m^{F7A/W11A}$, $CC2m^{\Delta\alpha1}$, and CC2m. The average binding free energies are marked out in (c)

regulating a plethora of biological activities in cell signaling. Regardless of the canonical CCs underpinned by seven-residue repeats (*abcdefg*) or noncanonical CCs formed by 11-residue, 15-residue, or 19-residue repeats (Ludwiczak et al., 2019), α1-helix is absent. This leads us to question what role the α1-helix does play in Bcr CC oligomerization. To explore the function of the α1-helix in the binary assembly of the Bcr CC domain, we simulated the binary systems with the F7A/W11A mutations in the small α1-helix ($CC2m^{F7A/W11A}$) and with the deletion of α1-helix ($CC2m^{\Delta\alpha1}$). We observed that due to the loss of the aromatic interactions between the α1-helix and α2-helix, the α1-helix encountered significant structural change, transforming the ordered helical into the random coil conformation (Figure 3a). Large fluctuations in the mutated α1-helix can be observed (Figure 3b). However, neither the α1-helix mutations nor deletion affected the α2–α2 packing posture and dynamics. Since the conformation of the α1-helix of one chain was not completely disrupted, chains A and B maintained strong binding in the $CC2m^{F7A/W11A}$ system, as evidenced by the low binding free energy (∼ − 141.3 kcal/mol), comparable to that of the CC2m system (Figure 3c). When the α1-helix is absent, the binding energy between the two chains in the $CC2m^{\Delta\alpha1}$ system increased to ∼ − 53.0 kcal/mol, mainly caused by the great increase of the molecular mechanics energy (Figure S3). However, the two α2 helices in the $CC2m^{F7A/W11A}$ and $CC2m^{\Delta\alpha1}$ systems maintained strong interactions. The monomer–monomer α2–α2 interaction energies in both systems peak at ∼ − 270 kcal/mol (Figure 3d), slightly higher than that of the CC2m system. These indicate that the α1 helices can assist the monomer–monomer binding but do not significantly affect the packing and interaction between the two α2 helices of the Bcr CC domain.

2.4 | Two surfaces of the binary Bcr CC

Upon dimerization, the binary Bcr CC yield two surfaces for tetramerization. Both have three hydrophilic blocks on the two α2 helices (Figure 4a). Each block contains two positively charged and two negatively charged residues, balancing the surface charge. These charged residues are involved in interchain and intrachain salt bridge formations. For Surface 1, both Blocks 1 and 3 are

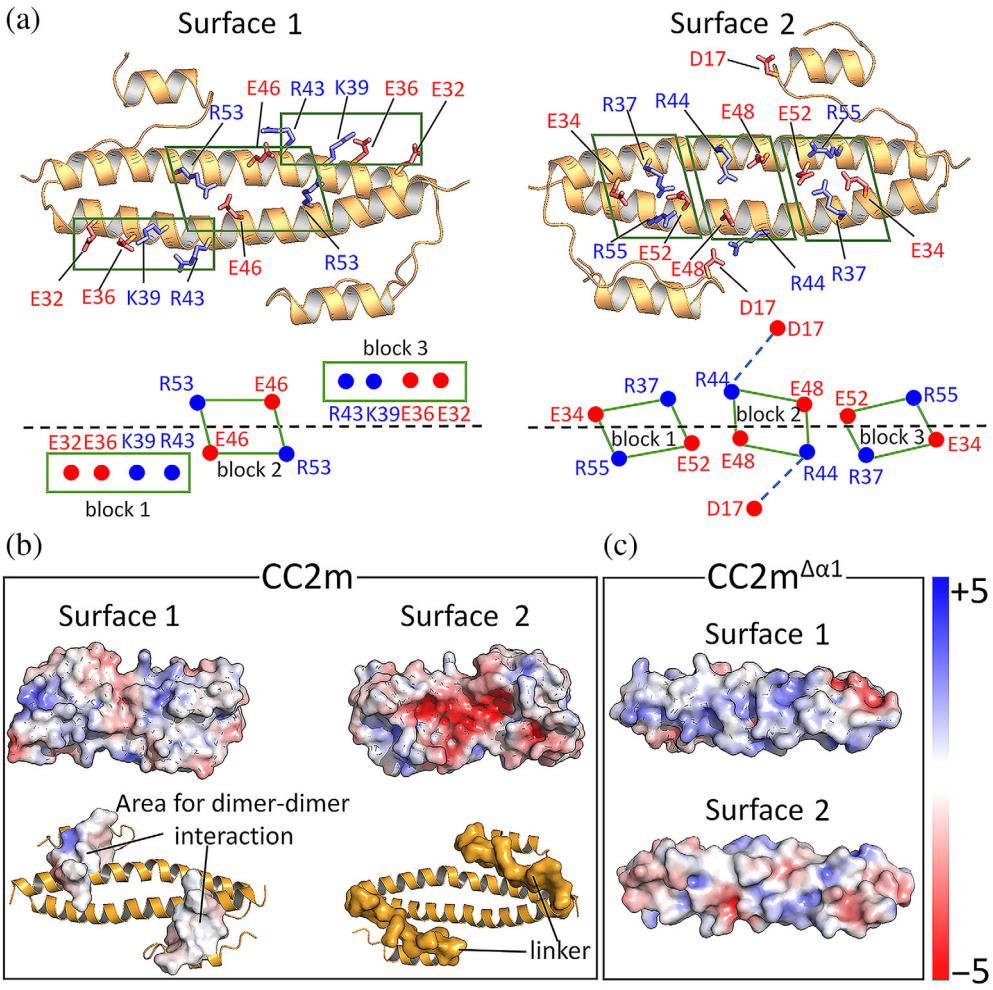

FIGURE 4 Two surfaces of the binary Bcr CC. (a) Hydrophilic blocks on Surfaces 1 and 2 of the binary unit of the Bcr CC domain. Each hydrophilic block contains two negatively charged residues and two positively charged residues. On Surface 2, D17 in linker$^{\alpha1-\alpha2}$ can form a salt bridge with R44 in the α2-helix, which disrupts charge balance of the surface. Electrostatic property of Surfaces 1 and 2 of the dimer for the systems of (b) CC2m and (c) CC2m$^{\Delta\alpha1}$. The color bar denotes the charge properties (red, negative charge; blue, positive charge). In (b), the two hydrophobic areas for the dimer–dimer interactions of Surface 1 and two areas of linker$^{\alpha1-\alpha2}$ of Surface 2 are highlighted

identical. Four residues, E32, E36, K39, and R43 in the two blocks face linearly along the axis of the α2-helix. Their corresponding regions in the opposite chain are relatively hydrophobic, assisting in the dimer–dimer α1–α2 interaction. Block 2 is an interacting area for the dimer–dimer packing, where E46 and R53 from the two chains display a cross-arrangement in which the two residues with the same charge property (positive or negative) are located at the diagonal points. For Surface 2, residues in all the three blocks show a cross-arrangement, same as Block 2 of Surface 1. Blocks 1 and 3 consist of the same residues of E34, R37, E52, and R55, in which E34 and R37 are from one chain, and E52 and R55 are from the other. Block 2 contains R44 and E48 from both chains. Two linkers connecting α1 and α2 are exposed on Surface 2. In Surface 2, these linkers produce steric hinderance, obstructing the accessibility of the surface. In addition, the charged residue D17 in the linker disrupts the charge balance of Block 2. D17 can form a salt bridge with R44 in Block 2, leading to negatively charged environment in the middle region of Surface 2 (Figure 4b). In the absence of the linker, the charge balance of surface can be restored (Figure 4c). This suggests that dimer–dimer packing is unfavorable through Surface 2 due to the steric hinderance and unbalanced charge on the linker surface. We speculate that in the absence of the α1-helix and linker, Surface 2 may contribute to the interaction. In this way, the Bcr CC domain probably forms higher-order oligomers in the manner of amyloid elongation.

2.5 | Salt bridges mediate monomer–monomer interaction in the binary Bcr CC

The charged residues in the blocks on each surface form interchain and intrachain salt bridges, mediating the monomer–monomer interaction of the binary complex. Mutations of these residues in the blocks can disrupt the charge balance and salt bridges, affecting the interchain interaction. For Surface 1, only Block 2 is responsible for the interchain interaction, whereas for Surface 2 all blocks participate in the interchain monomer–monomer

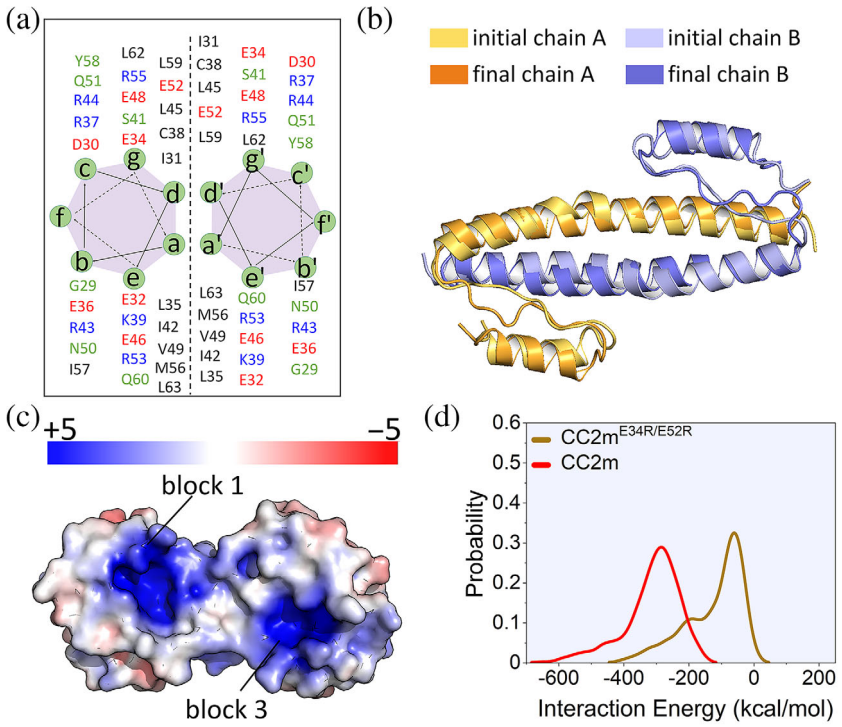

FIGURE 5 Salt bridges mediate monomer–monomer interaction in the binary Bcr CC. (a) α2–α2 interface (dash line) in the binary Bcr CC. The letters of *a*, *b*, *c*, *d*, *e*, *f*, and *g* indicate the residue positions in the α2-helix of one monomer, and *a*′, *b*′, *c*′, *d*′, *e*′, and *f*′ denote that of the other monomer. Residues in the α2-helix are mapped at the corresponding positions. The positively charged, negatively charged, polar, and hydrophobic residues are colored in blue, red, green, and gray, respectively. (b) Structural alignment of the final to initial configurations, (b) electrostatic property of Surface 2, and (c) probability distributions of the monomer–monomer α2–α2 interaction energy for the $CC2m^{E34R/E52R}$ and CC2m systems

interaction (Figure 4). It was reported that E48R substitution on the surface of Block 2 hindered the homo-oligomerization ability of the Bcr CC domain (Dixon et al., 2011, 2012). This can be explained by the charge reversal mutation which weakens the interchain α2–α2 interaction but increases the interaction with the linker, resulting in the disruption of the CC conformation. Here, we further consider mutations in Blocks 1 and 3 of Surface 2, since two interchain salt bridges, E34-R55 and R37-E52, and other two intrachain salt bridges, E52-R55 and E34-R37, are important for constituting the binary assembly of the Bcr CC domain (Figure 5a; Peiris et al., 2020). We simulated the systems with the E34R/E52R mutations and monitored stability of the binary complex. Interestingly, we observed that the interchain α2–α2 interaction appears to be favorable without significant change in the monomer–monomer packing within the simulation timescale (Figure 5b). Although no immediate dissociation of the complex was observed, E34R/E52R the mutations disrupted the charge balance and the salt bridges in Blocks 1 and 3 of Surface 2 (Figure 5c). The disruptions caused by the electrostatic repulsion in Blocks 1 and 3 weaken the interchain α2–α2 interaction, which may eventually dissociate the binary conformation. The interaction energy between the two populated α2 helices is ~ -80 kcal/mol, decreased by ~70% comparing to that for the wild-type system of CC2m (Figure 5d). This indicates that the salt bridges (or charge balance) in the blocks of Surface 2 play a critical role in the binary assembly of the Bcr CC domain.

2.6 | α1-helix is required for specific packing of two binary Bcr CCs in the quaternary complex

The quaternary complex of the Bcr CC domain displays a crossed packing topology with a crossing angle of ~130° between the two binary Bcr CCs (Figure 1b). This crossed packing conformation is unique and remarkably different from most other CC species that adopt a helical-wheel configuration when they aggregate into higher-order oligomers (Apostolovic et al., 2010; Utterstrom et al., 2021). In the crossed packing, two binary Bcr CCs adopt the dimer–dimer α1–α2 and α2–α2 interactions. To determine the role of the α1-helix in the quaternary assembly of the Bcr CC domain, we simulated the quaternary systems with the F7A/W11A mutations in the small α1-helix ($CC4m^{F7A/W11A}$) and with deletion of α1-helix ($CC4m^{\Delta\alpha1}$). Our simulations showed that $CC4m^{F7A/W11A}$ appears to preserve the initial crossed packing conformation, while $CC4m^{\Delta\alpha1}$ disrupts the initial configuration (Figure 6a). When compared with the wild-type CC4m system, both $CC4m^{F7A/W11A}$ and $CC4m^{\Delta\alpha1}$ systems increased the dimer–dimer α2–α2 contact area (Figure S4), due to the loss of the crossed packing propensity resulting from unstable or absent of the α1-helix interaction. This is apparent in the $CC4m^{\Delta\alpha1}$ system where in the absence of the dimer–dimer α1–α2 interaction, two binary Bcr CCs are aligned in parallel to each other, dramatically increasing the dimer–dimer α2–α2 contact area. For $CC4m^{F7A/W11A}$, although the dimer–

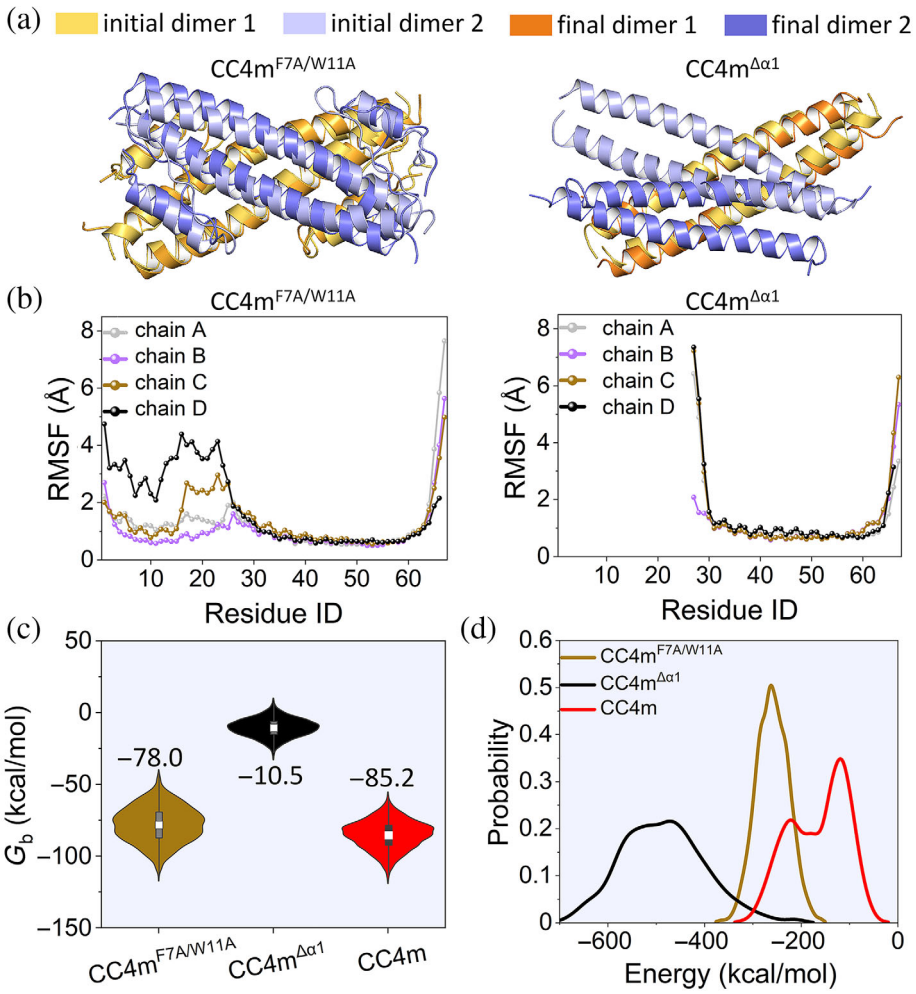

FIGURE 6 α1-helix is required for specific packing of two binary Bcr CCs in the quaternary complex. (a) Structural alignment of the final to initial configurations, (b) RMSFs of chains A, B, C, and D, (c) binding free energy, $< G_b >$, and (d) probability distributions of the dimer–dimer α2–α2 interaction energies for the three systems of $CC4m^{F7A/W11A}$, $CC4m^{\Delta\alpha1}$, and CC4m. The average binding free energies are marked out in (c)

dimer α1–α2 interaction may protect the helicity of the α1-helix, disruption of the monomer–monomer α1–α2 aromatic interactions in the binary units caused large fluctuations of the α1-helices (Figure 6b). The changes in the dimer–dimer α2–α2 cross-packing increased the stability of the quaternary assembly, resulting in the increased binding free energy for the interaction between two binary CCs, which are ∼ − 78.0 and ∼ −10.5 kcal/mol for $CC4m^{F7A/W11A}$ and $CC4m^{\Delta\alpha1}$, respectively (Figure 6c). For $CC4m^{\Delta\alpha1}$, the remarkable change of packing of the binary units toward the parallel orientation greatly increased the solvation energy barrier (Figure S5), causing 87.7% increase of the binding free energy relative to the wild-type system. This indicates that the α1-helix can constrain the orientation of the two binary Bcr CCs favorable for the cross-packing. The dimer–dimer α2–α2 interaction energies for $CC4m^{F7A/W11A}$ and $CC4m^{\Delta\alpha1}$ peak at ∼ − 260.0 and ∼ −490 kcal/mol, respectively (Figure 6d), lower than ∼ − 110.0 kcal/mol for the CC4m system. This may be attributed to the increase of the dimer–dimer α2–α2 contact area. Based on the above observations, we concluded that the α1-helix is the determinant for the specific packing between the binary units in the quaternary assembly of the Bcr CC domain.

2.7 | Salt bridges mediate the interaction of binary Bcr CCs in the quaternary complex

Surface 1 of the binary Bcr CC is favorable for the dimer–dimer interaction to form the quaternary complex. Block 2 plays a major role, since E46 and R53 at position *e* contribute to the strong electrostatic interaction through salt bridge formations (Figure 7a). To demonstrate the importance of the interaction in the middle region for Bcr CC tetramerization, we simulated the quaternary systems with three-residue mutations of E34R/E46R/E52R ($CC4m^{E34R/E46R/E52R}$) and one-residue mutation of E46R ($CC4m^{E46R}$). Considering that the α1-helix is critically important for the dimer–dimer interaction, an additional mutant system of E46R with deletion of the α1-helix ($CC4m^{\Delta\alpha1/E46R}$) was also simulated. Due to the

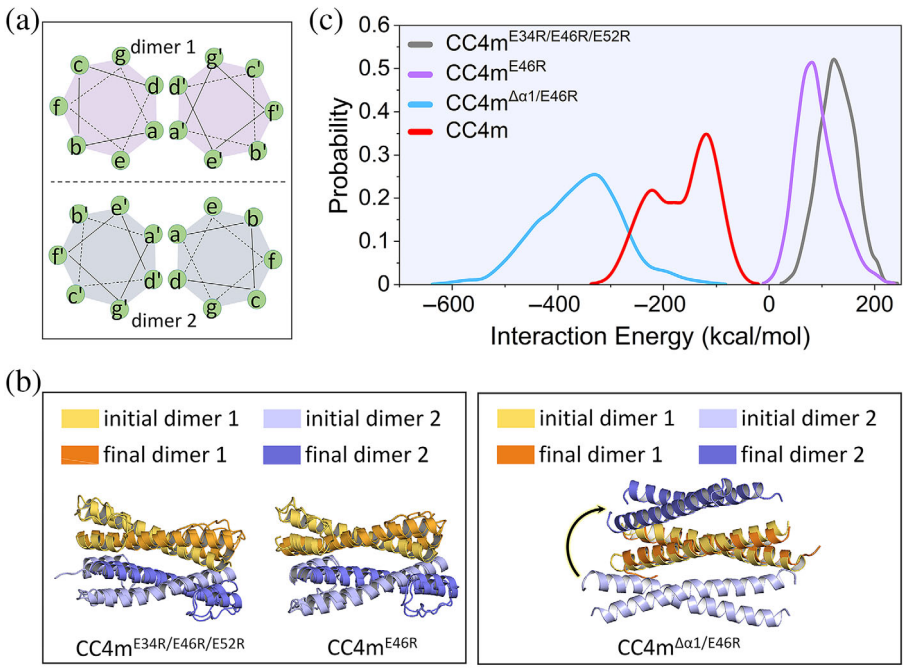

FIGURE 7 Salt bridge mediates the interaction of binary Bcr CCs in the quaternary complex. (a) Dimer–dimer α2–α2 interface (dash line) in the quaternary Bcr CC. (b) Structural alignment of the final to initial configurations and (c) probability distributions of the dimer-–dimer α2–α2 interaction energies for the CC4m$^{E34R/E46R/E52R}$, CC4m^{E46R}, CC4m$^{\Delta\alpha1/E46R}$, and CC4m systems

restriction of the α1-helix, no immediate dissociation and conformational change for both CC4m$^{E34R/E46R/E52R}$ and CC4m^{E46R} systems were observed (Figure 7b). However, the dimer–dimer α2–α2 interaction energies of both mutant systems exhibit positive distributions (Figure 7c), indicating that electrostatic repulsive force in the middle region results in the unfavorable dimer–dimer α2–α2 interaction. The dimer–dimer α2–α2 interaction energy for CC4m$^{E34R/E46R/E52R}$ shows more positive distribution comparing to CC4m^{E46R}, suggesting that weakened monomer–monomer α2–α2 interaction can further weaken the dimer–dimer α2–α2 interaction. For CC4m$^{\Delta\alpha1/E46R}$, without the α1-helix restriction, the dimer–dimer interface was destroyed, yielding one binary CC migrating to interact with Surface 2 of the other binary CC (Figure 7b). The distribution of the dimer–dimer α2–α2 interaction energy for CC4m$^{\Delta\alpha1/E46R}$ accumulate at ~ -320 kcal/mol (Figure 7c), weaker than that for the system without the mutation, CC4m$^{\Delta\alpha1}$. This indicates that without the α1-helix, the two surfaces of the binary Bcr CC likely participate in the interaction, which may lead to higher-order Bcr CC oligomerization. This also confirms that the α1-helix is required for the specific packing of the Bcr CC quaternary complex.

3 | DISCUSSION

Oligomerization of the N-terminal CC domain of the Bcr-Abl oncoprotein is essential for its tyrosine kinase activity that drives different leukemias, especially CML. In this work, we depict the oligomerization steps through comprehensive analysis and tests of key parameters that regulate the process at the atomic level. Our observations determine that the oligomerization is a distinct stepwise process (Figure 8). It initiates with the dimerization, where it forms a binary assembly. The monomer–monomer α2–α2 hydrophobic interaction is the driving force for Bcr CC dimerization. The interchain α1–α2 aromatic interaction assists in the monomer–monomer packing. Upon dimerization, the Bcr CC dimer generates two surfaces. Surface 1 is favorable for the dimer–dimer interaction that forms the quaternary complex. This is not the case for Surface 2, where the exposed linker$^{\alpha1-\alpha2}$ induces steric hindrance and destroys the charge balance, leading to its inaccessibility. Consequently, Surface 2 does not favor the dimer–dimer interaction. This may be the primary reason why the Bcr CC domain cannot form higher-order oligomers. The quaternary Bcr CC presents a unique dimer–dimer packing with a crossing angle of ∼130° between the CC axes of one dimeric unit and the other (Figure S1). In the quaternary complex, the dimer–dimer α1–α2 hydrophobic interaction restricts the packing orientation of the binary assemblies and contributes primarily to the dimer–dimer packing. The dimer–dimer α2–α2 salt bridges network in the middle region favors it.

In the oligomerization of the Bcr CC domain, the binary assembly serves as the basic building unit for quaternary complex formation. The packing of the binary and quaternary assemblies of the Bcr CC domain preserved structural stability. From the energetic perspective, the monomer–monomer interface is much stronger

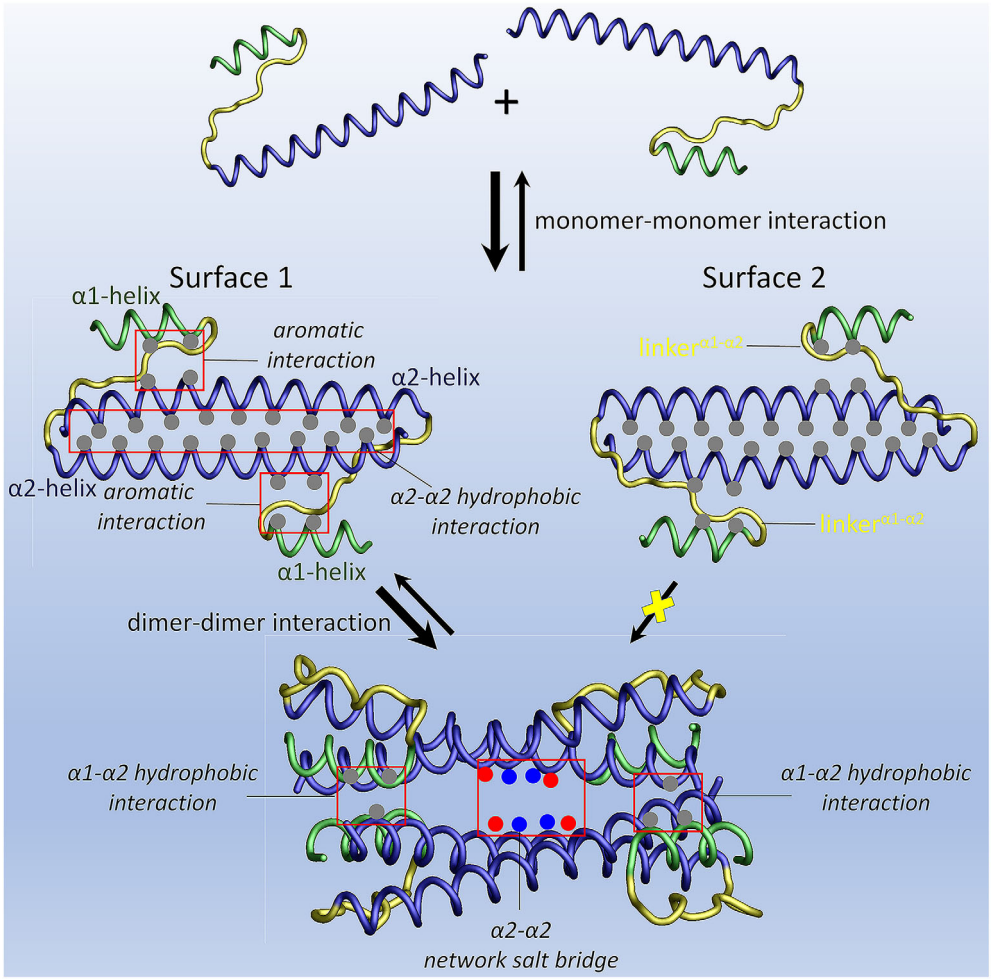

FIGURE 8 Schematic diagram for the oligomerization mechanism of the Bcr CC domain. Oligomerization of the Bcr CC domain is a stepwise process. It initiates with dimerization, yielding a binary assembly. In the binary Bcr CC, the monomer–monomer α2–α2 hydrophobic interaction dominates the dimer packing, while the monomer–monomer α1–α2 aromatic interaction assists in the packing stability. Upon dimerization, the binary Bcr CC yields two surfaces. Surface 1 contributes to the dimer–dimer packing, while Surface 2 lacks an interaction ability owing to steric hindrance and unbalanced charge caused by linker$^{\alpha1-\alpha2}$. Two binary assemblies of the Bcr CC domain pack crossly with each other, forming a quaternary assembly. In the quaternary Bcr CC, the dimer–dimer α1–α2 hydrophobic interaction determines the specific dimer–dimer packing, while the dimer–dimer α2–α2 network salt bridges in the middle region aid it

than the dimer–dimer interface, indicating that dimer–dimer disruption is easier than monomer–monomer disruption. Our results identify different roles that the α1-helix plays in the binary and quaternary assembly of the Bcr CC domain. It assists but is not required for the monomer–monomer packing. However, helix α1 is the determinant for the specific dimer–dimer packing of the quaternary formation. The α1-helix restricts the packing orientation of the two binary assemblies in the quaternary complex and guards against their dissociations through the dimer–dimer α1–α2 hydrophobic interaction. For the quaternary complex in the absence of the α1-helix, the two binary Bcr CCs tend to be aligned in parallel (Figure 6a). If the α1-helix is not involved in the packing, the parallel quaternary α2/α2–α2/α2 packing is less stable, eventually dissociating into two binary complexes. Without the specific cross-wise packing in the quaternary complex, the concentration of Bcr-Abl is decreased at the membrane, which weakens the trans-autophosphorylation. A blotting assay has shown that the Bcr CC domain can form dimer, trimer, and tetramer in vitro (Mcwhirter et al., 1993). As time progresses, the assay showed that the dimer signal weakened, while that of the tetramer strengthened, indicating that the Bcr dimer further assembled into the tetramer. This supports our observation. There was no significant change of the signal for the Bcr trimer in the assay. Our ternary complex models were constructed based on the crystal structure of the quaternary complex. Although the ternary complex did not point to dissociation (Figure 2a), the

interfaces may not be the most favorable. Based on the sequence similarity of the α2-helix with other CC domains, one possible assembly mode is the helical-wheel packing, in which the α1-helix may not participate in the packing.

Salt bridges formed by residues at the *g* and *e* positions mediate both the binary and quaternary packings of the Bcr CC domain. The necessity of salt bridges in the Bcr CC domain has been implicated in the activation of Bcr-Abl, and Bcr-FGFR1, another Bcr-fused protein (Peiris et al., 2020). Salt bridges in the blocks of Surface 2 help the monomer–monomer interaction (Figure 4a). The reverse charge mutations, E34R and E52R, can destroy the salt bridges of Surface 2 and weaken the monomer–monomer interaction. The two mutations significantly abrogated Bcr-FGFR1's cell transformation (Peiris et al., 2020). The network of salt bridges formed by residues in Block 2 of Surface 1 serves to assist the dimer–dimer interaction. The E46R mutation disfavors the dimer–dimer α2–α2 interaction. Combination of deletion of the α1-helix and the E46R mutation completely broke the dimer–dimer interaction, but Surface 2 was involved in a new dimer–dimer interaction. This suggests that if Surface 1 is unavailable (e.g., already occupied by the dimer–dimer interaction), Surface 2 might be available for the higher-order oligomers. Here we observe that the three mutations, E34R, E52R, and E46R, can disturb both the monomer–monomer and dimer–dimer interfaces. Combining E46R with E34R/E52R in the Bcr region executes enhanced transforming activity of the Bcr-fused oncoprotein (Peiris et al., 2020). Our data showed that the linker connecting helices α1 and α2 (linker$^{\alpha1-\alpha2}$) prevents Surface 2 of the Bcr CC domain from a dimer–dimer interaction in two ways: (i) the linkers can elicit steric hinderance, and (ii) the charged D17 in the linker disrupts the charge balance of Block 2, leading to negatively charged environment in the middle region of Surface 2. This is further supported by the observations of restoration of the charge balance of Surface 2 in the CC2m$^{\Delta\alpha1}$ system (Figure 4c) and migration of one dimer to interact with Surface 2 of the other dimer in the CC4m$^{\Delta\alpha1/E46R}$ system (Figure 7b). These observations lead us to speculate that in the absence of the α1-helix, the tetrameric form will not terminate the aggregation. Instead, the α2 helices may aggregate into different oligomeric forms, such as the helical-wheel packing as observed in some other CCs (Apostolovic et al., 2010; Lupas et al., 2017; Utterstrom et al., 2021), or the dimer–dimer stacking form resembling one mode of amyloid aggregation—amyloid elongation (Figure 9; Gurry & Stultz, 2014; Jang et al., 2014; Ma & Nussinov, 2012; Ren et al., 2018; Zhang, Zhang, et al., 2021).

Fused Bcr is a part of the Bcr-Abl oncoprotein. Interactions of the Bcr CC domain can promote Bcr-Abl oligomerization. The autophosphorylation of Bcr-Abl with ablation of the CC domain in 32D cells was dramatically reduced as compared with that of wt Bcr-Abl (He et al., 2002; Zhang et al., 2001), indicating oligomerization of the Bcr CC domain can provide a favorable microenvironment for Bcr-Abl accessing the substrate and executing its tyrosine kinase activity. Structurally, the two monomers are antiparallel to each other in the binary assembly of the Bcr CC domain, resulting in the relatively long distance (∼60 Å) between the two edges of C-termini. As long as two binary Bcr CCs assemble together forming a quaternary complex, the opposite C-termini across the dimer–dimer interface are brought into a closer proximity with a shorter distance (∼24 Å; Zhao et al., 2002). This can improve the trans-autophosphorylation of Bcr-Abl. In terms of the biology, Bcr-Abl has multiple substrates except for itself. Activated Bcr-Abl can phosphorate the tyrosine residues of itself (e.g., Y177 in the Bcr region and Y1294 in the Abl region; Cilloni & Saglio, 2012; Liu, Jang, et al., 2022) and downstream signaling proteins, such as Crk, Crk-Like (CrkL), focal adhesion kinase 2 (FAK2), the LIM, and SH3 domain protein 1 (Colicelli, 2010; Frietsch et al., 2014; La Rosee et al., 2008). If one Bcr-Abl phosphorylates another substrate, the other can still phosphorylate Y177 in the Bcr region and Y1294 in the Abl region. Phosphorylation and dephosphorylation occur frequently in cells. As long as the substrate is dephosphorylated, Bcr-Abl molecules accumulating on the membrane can efficiently phosphorylate the substrate. pY177 in Bcr-Abl is the GRB2 SH2 domain binding site (Liu, Jang, et al., 2022). Binding activates the Ras/MAPK pathway, promoting cell proliferation. High concentration of Bcr-Abl on the membrane can rescue pY177 phosphorylation, leading to sustainable Ras/MAPK signaling. Disruption of the CC oligomerization is expected to reduce Bcr-Abl clustering on the membrane, thus activation of its substrates.

An inhibitor obstructing CC oligomerization can thus serve either as the main therapy or in combination, collaborating with TKIs of the Abl kinase domain. An efficient inhibitor would leverage a strong ability to favor hetero-oligomerization and minimum probability of homo-oligomerization (Ben-Tal & Lupas, 2021). Rationally replacing residues at the *g* and *e* positions should be able to (i) disrupt an existing salt bridge, thus disturbing the association stability, or (ii) introduce additional salt bridges, enhancing the packing. A grasp of the key residues that regulate the structure, packing stability, and interaction of the Bcr CC domain is thus vastly important for designing an inhibitor against the Bcr CC interfaces.

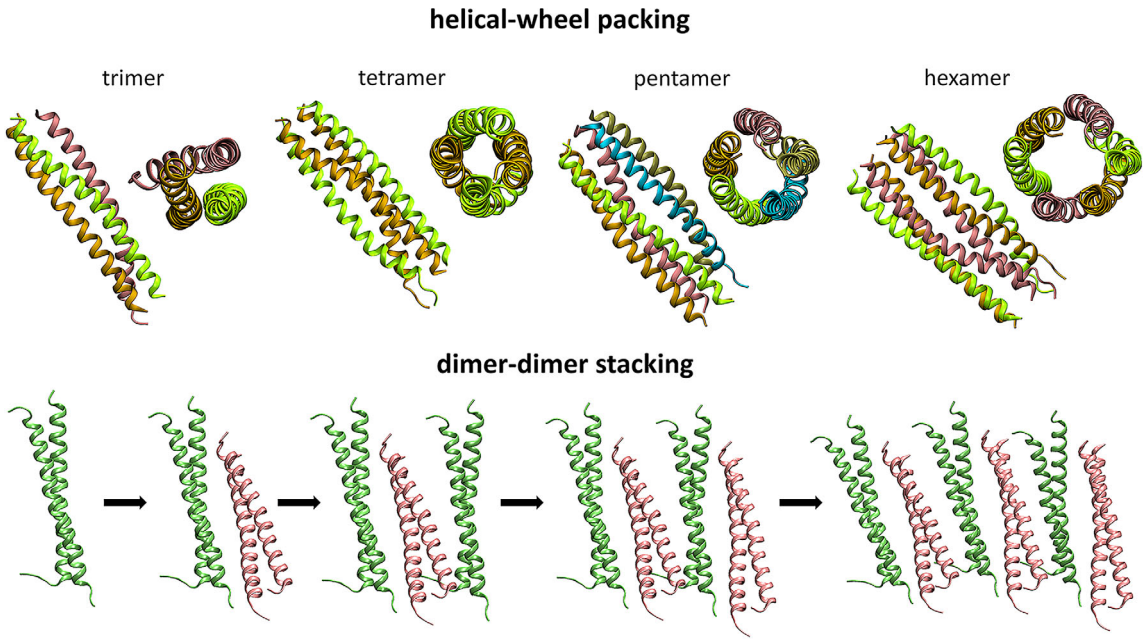

FIGURE 9 Proposed aggregation of the Bcr CC domain when the α1-helix is absent. In the absence of the α1-helix, the α2 helices of the Bcr CC domain are likely to aggregate into different oligomeric forms. Like other CC species, the α2 helices may assemble into both odd-numbered and even-numbered aggregates in the helical-wheel manner. If the dimeric unit of the Bcr CC domain in the absence of the α1-helix is the building block of the Bcr CC oligomers, both Surfaces 1 and 2 participate in the dimer–dimer interaction. The α2 helices aggregate into even-numbered oligomers through the dimer–dimer stacking resembling amyloid elongation

Lim's group (Dixon et al., 2011) identified S41 and Q60 as the positions to form salt bridges with residues E32 and E48, respectively. Substitutions of S41R and Q60E are expected to enhance the monomer–monomer interfaces of the binary Bcr CC. An efficient inhibitor should be competitive to interactions of the CC domain but have relatively weaker ability to homo-oligomerize. Mutations that weaken the interfaces should also be considered when designing an inhibitor. The mutations of L45D and E48R fulfill this aim. Lim's group introduced two Bcr CC mutants (CCmut2 and CCmut3) that involve these mutations (S41R, L45D, E48R, and Q60E; Dixon et al., 2011, 2012). The two mutants exhibited desirable hetero-oligomeric, and not homo-oligomeric properties, and efficiently oligomerized with Bcr-Abl, thus significantly reducing the Bcr-Abl activity and cell proliferation. In this work, we identified E34R/E52R and E46R mutations are able to weaken the monomer–monomer and dimer–dimer interfaces, respectively. Combined with earlier experiments, a Bcr CC-derived inhibitor that contains the mutations of S41R, Q60E, E34R, E48R, E52R, E46R appears a promising inhibitor of Bcr-Abl oligomerization. This can guide inhibitor design targeting the Bcr-Abl CC domains. Experimentally, it suggests that using the Bcr CC domain sequence (residues 1–63) with the mutations of S41R, Q60E, E34R, E48R, E52R, E46R may serve as an inhibitor to Bcr-Abl oligomerization (Beissert et al., 2003, 2008; Bruno & Lim, 2015; Dixon et al., 2011, 2012; Woessner et al., 2015).

The efficacy of a small molecule drug can be evaluated according to its capability to bind and interact with its selective targets. This process is fast and reversible. Long duration of drug binding is expected to elicit therapeutic response (Ung et al., 2019). The oligomeric protein–protein interaction (PPI) interface of the Bcr-Abl CC domain might be blocked by an irreversible covalent drug. Covalent linkage of a small molecule to the protein surface to block the endogenous PPIs has advanced drug design (Sutanto et al., 2020). Currently, covalent inhibitors account for 30% of the drug market. Some residues, including Cys, Ser, Thr, Tyr, His, and Lys, have been identified as covalent targets for drug warhead (Bum-Erdene et al., 2020; Gambini et al., 2019; Gehringer & Laufer, 2019; Poirier, 2021). A potential alternative strategy to inhibit Bcr CC dimerization (or tetramerization) is using a covalent inhibitor to block the monomer–monomer (or dimer–dimer) interface. C38 is located at the monomer–monomer interface and S41 is adjacent to the interface (Figure S6). Both are options to be covalently linked by small molecules to interfere with the dimer interface of the Bcr CC domain. K39, T61, and K65 are nearby the dimer–dimer interaction areas. Drug covalently bonding to them may inhibit the association between two binary Bcr CCs. Bivalent drugs that link

these residues in the Bcr-Abl CC domain to other domains could also be promising candidates in quenching the homo-oligomerization of the Bcr-Abl, and its membrane clustering (Liu et al., 2010).

4 | CONCLUSIONS

In summary, here we determined the oligomerization process of the Bcr CC domain and clarified questions that it raised. We addressed the questions that we posed upfront. We elucidated the functions of the α1-helix in the monomer–monomer packing for binary assembly and the dimer–dimer packing for quaternary assembly, and exactly what leads to the specific packing of the Bcr CC tetramer. We also explained why the Bcr CC domain favors the quaternary complex in the form of dimer–dimer packing and why its higher-order oligomeric assemblies cannot be formed. We described the key parameters that control dimerization and tetramerization of the Bcr CC domain and detailed the stepwise oligomerization process, which can be exploited to design high-efficiency inhibitors against Bcr-Abl homo-oligomerization or clustering.

Oligomerization initiates with dimerization, producing a binary assembly. The binary Bcr CC serves as the building block for tetramerization of the Bcr CC domain. Upon dimerization, the binary Bcr CC yields two surfaces. Surface 1 participates in the dimer–dimer packing, while Surface 2 lacks an interaction ability due to steric hindrance and unbalanced charge caused by the linker$^{\alpha1-\alpha2}$. This results in the Bcr CC domain oligomerization terminating with a quaternary assembly. We identify the small α1-helix and salt bridges as the regulators of the Bcr CC domain oligomerization. For the binary Bcr CC, the hydrophobic α2–α2 interaction dominates the monomer–monomer packing, the α1-helix assists in packing stability, and salt bridges of Surface 2 mediate the monomer–monomer interface. For the quaternary Bcr CC, the α1-helix is required for the specific dimer–dimer packing and salt bridges in the middle region of Surface 1 assist it.

Oligomerization of the Bcr CC domain increases the concentration of Bcr-Abl on the membrane. This leads to Bcr-Abl efficiently phosphorylating itself and other substrates, and makes disruption of Bcr-Abl assemblies a promising strategy for mitigating Bcr-Abl activity in CML. Identification of E34R/E52R and E46R mutations as weakening the monomer–monomer and dimer–dimer interfaces, respectively, suggests that a Bcr CC-derived inhibitor that contains the mutations of S41R, Q60E, E34R, E48R, E52R, and E46R is promising as an inhibitor of oligomerization which can combine with TKI and allosteric drugs that target the ATP pocket. Altogether, the strategy outlined here based on comprehensive mechanistic analysis can combine with orthosteric and allosteric TKI, assisting in countering emerging drug resistance in CML.

5 | MATERIALS AND METHODS

5.1 | Preparing the Bcr CC domain complexes

The crystal structure of Bcr-Abl oncoprotein oligomerization (PDB: 1K1F) was used to model the binary, ternary, and quaternary assemblies of Bcr CC domain. A binary system (CC2m), two ternary systems (CC3m1 and CC3m2), and a quaternary system (CC4m) were constructed (Table S1). CC2m contains chains A/B. CC3m1 and CC3m2 involve chains A/B, C and A/B–D, respectively. CC4m contains chains A/B-C/D. In addition, the mutations, F7A and W11A, in the small α1-helix for the binary (CC2m$^{F7A/W11A}$) and quaternary (CC4m$^{F7A/W11A}$) systems, and the deletion of α1-helix, Δα1, for the binary (CC2m$^{\Delta\alpha1}$) and quaternary (CC4m$^{\Delta\alpha1}$) systems were also considered. We further obtained four additional systems with the mutations, E34R, E46R, and E52R, in the long α2-helix combined with the α1 deletion for the binary (CC2m$^{E34R/E52R}$) and quaternary (CC4m$^{E34R/E46R/E52R}$, CC4m^{E46R}, and CC4m$^{\Delta\alpha1/E46R}$) systems. A total of 12 systems were constructed and solvated using the TIP3P model. Na^+ and Cl^- were inserted to neutralize the systems and to obtain a physiological salt concentration near 150 mM. Depending on the systems, numbers of ions added to the systems were varied. The production simulations were run for a period of 2 μs for each system.

5.2 | MD simulation protocols

All simulations were carried out according to our previously published protocol (Jang et al., 2021; Liu, Jang, et al., 2022; Maloney et al., 2021; Zhang et al., 2019; Zhang, Jang, et al., 2021). The protocol details are as follows. Prior to the productions runs, a series of minimization and dynamics cycles were performed, ensuring that bad atom contacts were removed in the Bcr systems. The productions runs were performed under the NPT ensemble (constant number of atoms, pressure, and temperature). 3D periodic boundary conditions were applied to each system, using NAMD 2.13 package (Phillips et al., 2005) with CHARMM (Brooks et al., 2009) all-atom force field (version 36 m; Huang et al., 2017; Klauda et al., 2010). The pressure was retained at 1 atm using the

Langevin piston control algorithm. The temperature at 310 K was maintained using the Langevin thermostat method with a damping coefficient of 1 ps^{-1}. All covalent bonds including hydrogen atoms were constrained using the SHAKE algorithm. The velocity Verlet algorithm was used to integrate the Newton motion equation with time step of 2 fs. The long-range electrostatic interactions between atoms were calculated by the particle mesh Ewald method with a grading space of 1.0 Å. The short-range van der Waals (vdW) interactions were calculated using switching functions with the twin-range cutoff at 12 and 14 Å. Trajectories of the atom coordinates were collected every 2 ps for analysis. The analysis was implemented with the CHARMM (version c45b1; Brooks et al., 2009) and VMD packages based on the FORTRAN and TCL scripts. Averages were also taken over from the last 1 μs trajectories.

5.3 | Binding free energy calculations

Different in silico methods are available for estimating binding free energy of protein–protein interactions, including implicit and explicit solvent models (Wang et al., 2019). In implicit solvent models, the solvent is usually regarded as unstructured continuum. Herein, the explicit atomic descriptions of solvent are ignored, such as hydrogen bonds between the solute and the solvent (Zhang, Zhang, et al., 2017). This leads to overstabilization of salt bridges and hydrogen bonds within the solute, incorrect ion distribution, and unphysical sampling. The solvent-based entropic effects are left out. However, considering that explicit solvent molecules account for a large number of atoms in the simulation systems, the number of degrees of freedom and interactive particles of the system are reduced in implicit solvent model. The conformational search of the solute is faster as compared with explicit solvent models. Implicit solvent models are practical for the time-consuming systems, such as protein–protein interaction and drug binding systems. In this work, the binding free energies between two monomers in the binary system, between dimer and monomer in the ternary system, and between two dimers in the quaternary system were calculated by the algorithm of an implicit solvent model, the MM-GBSA, within the CHARMM program (version c45b1; Brooks et al., 2009) . In the calculation, we followed our earlier protocol (Jang et al., 2016, 2017, 2019; Liao et al., 2018; Ozdemir et al., 2018; Weako et al., 2021; Zhang, Jang, et al., 2017). The molecular mechanics energy and the solvation energy were calculated in the GBSW module. In GBSW module, we specified 0.3 for SW, 0.003 for SGAMMA, 50 for NANG, 1.5 for DGP, 310 for TEMP, and 0.1 for CONC. Values for other parameters are default. The average binding free energy, $\langle \Delta G_b \rangle$, for the complex formation is a sum of the gas-phase contribution from the molecular mechanics energy $\langle \Delta E_{MM} \rangle$, the solvation energy contribution $\langle \Delta G_{sol} \rangle$, and the entropy contribution $T\Delta S$,

$$\langle \Delta G_b \rangle = \langle \Delta E_{MM} \rangle + \langle \Delta G_{sol} \rangle - T\Delta S,$$

where the angle brackets indicate the average along the last half of the simulations. The gas-phase contribution is a sum of the internal energy ΔH_{inter}, the electrostatic interaction ΔH_{elec}, and the vdW interaction ΔH_{vdW},

$$\Delta E_{MM} = \Delta H_{inter} + \Delta H_{elec} + \Delta H_{vdW}.$$

The solvation contribution is a sum of the electrostatic and nonpolar contribution, obtained from the GB calculation using the GBSW module (Im et al., 2003),

$$\Delta G_{sol} = \Delta G_{sol}^{elec} + \Delta G_{sol}^{nonpolar}.$$

The entropic term can be divided into the translational, rotational, and vibrational contributions,

$$T\Delta S = T\Delta S_{trans} + T\Delta S_{rot} + T\Delta S_{vib}.$$

We estimated the translational and rotational components from the principal moment of inertia and calculated the vibrational entropy using the quasiharmonic mode in the VIBRAN module of the CHARMM program (Brooks et al., 2009). The change in binding free energy due to the binary, ternary, or quaternary complex formation can be calculated using the equation,

$$\Delta G_b = G_b^{complex} - \left(G_b^{segment1} + G_b^{segment2} \right),$$

where the segment can be monomer or dimer.

AUTHOR CONTRIBUTIONS

Yonglan Liu: Conceptualization (lead); data curation (lead); formal analysis (lead); investigation (lead); methodology (equal); validation (lead); visualization (lead); writing – original draft (lead); writing – review and editing (lead). **Mingzhen Zhang:** Conceptualization (equal); formal analysis (supporting); investigation (supporting); resources (equal); software (equal); validation (equal); visualization (equal); writing – review and editing (equal). **Hyunbum Jang:** Conceptualization (equal); investigation (supporting); methodology (equal); resources (supporting); software (equal); validation

(supporting); visualization (supporting); writing – review and editing (equal). **Ruth Nussinov:** Conceptualization (equal); funding acquisition (lead); project administration (lead); resources (lead); software (equal); supervision (lead); validation (equal); visualization (equal); writing – review and editing (equal).

ACKNOWLEDGMENTS

This project has been funded in whole or in part with federal funds from the National Cancer Institute, National Institutes of Health (NHI), under contract HHSN261201500003I. The content of this publication does not necessarily reflect the views or policies of the Department of Health and Human Services, nor does mention of trade names, commercial products, or organizations imply endorsement by the U.S. Government. This research was supported [in part] by the Intramural Research Program of the NIH, National Cancer Institute, and CCR. The calculations had been performed using the high-performance computational facilities of the Biowulf PC/Linux cluster at the National Institutes of Health, Bethesda, MD (https://hpc.nih.gov/).

CONFLICT OF INTEREST

The author declares that there is no conflict of interest that could be perceived as prejudicing the impartiality of the research reported.

ORCID

Ruth Nussinov https://orcid.org/0000-0002-8115-6415

REFERENCES

Alves R, Goncalves AC, Rutella S, Almeida AM, De Las Rivas J, Trougakos IP, et al. Resistance to tyrosine kinase inhibitors in chronic myeloid leukemia-from molecular mechanisms to clinical relevance. Cancers (Basel). 2021;13:4820.

Apostolovic B, Danial M, Klok HA. Coiled coils: Attractive protein folding motifs for the fabrication of self-assembled, responsive and bioactive materials. Chem Soc Rev. 2010;39:3541–75.

Astl L, Verkhivker GM. Atomistic modeling of the ABL kinase regulation by allosteric modulators using structural perturbation analysis and community-based network reconstruction of allosteric communications. J Chem Theory Comput. 2019;15:3362–80.

Beissert T, Hundertmark A, Kaburova V, Travaglini L, Mian AA, Nervi C, et al. Targeting of the N-terminal coiled coil oligomerization interface by a helix-2 peptide inhibits unmutated and imatinib-resistant BCR/ABL. Int J Cancer. 2008;122:2744–52.

Beissert T, Puccetti E, Bianchini A, Guller S, Boehrer S, Hoelzer D, et al. Targeting of the N-terminal coiled coil oligomerization interface of BCR interferes with the transformation potential of BCR-ABL and increases sensitivity to STI571. Blood. 2003;102:2985–93.

Ben-Tal N, Lupas AN. Editorial overview: Sequences and topology: 'paths from sequence to structure'. Curr Opin Struct Biol. 2021;68:vi–viii.

Brooks BR, Brooks CL 3rd, Mackerell AD Jr, Nilsson L, Petrella RJ, Roux B, et al. CHARMM: The biomolecular simulation program. J Comput Chem. 2009;30:1545–614.

Bruno BJ, Lim CS. Inhibition of bcr-abl in human leukemic cells with a coiled-coil protein delivered by a leukemia-specific cell-penetrating peptide. Mol Pharm. 2015;12:1412–21.

Bum-Erdene K, Liu D, Gonzalez-Gutierrez G, Ghozayel MK, Xu D, Meroueh SO. Small-molecule covalent bond formation at tyrosine creates a binding site and inhibits activation of Ral GTPases. Proc Natl Acad Sci U S A. 2020;117:7131–9.

Caillat C, Fish A, Pefani DE, Taraviras S, Lygerou Z, Perrakis A. The structure of the GemC1 coiled coil and its interaction with the geminin family of coiled-coil proteins. Acta Crystallogr D Biol Crystallogr. 2015;71:2278–86.

Chen M, Turhan AG, Ding H, Lin Q, Meng K, Jiang X. Targeting BCR-ABL+ stem/progenitor cells and BCR-ABL-T315I mutant cells by effective inhibition of the BCR-ABL-Tyr177-GRB2 complex. Oncotarget. 2017;8:43662–77.

Chernyatina AA, Nicolet S, Aebi U, Herrmann H, Strelkov SV. Atomic structure of the vimentin central alpha-helical domain and its implications for intermediate filament assembly. Proc Natl Acad Sci U S A. 2012;109:13620–5.

Cilloni D, Saglio G. Molecular pathways: BCR-ABL. Clin Cancer Res. 2012;18:930–7.

Colicelli J. ABL tyrosine kinases: Evolution of function, regulation, and specificity. Sci Signal. 2010;3:re6.

Dixon AS, Miller GD, Bruno BJ, Constance JE, Woessner DW, Fidler TP, et al. Improved coiled-coil design enhances interaction with Bcr-Abl and induces apoptosis. Mol Pharm. 2012;9:187–95.

Dixon AS, Pendley SS, Bruno BJ, Woessner DW, Shimpi AA, Cheatham TE III, et al. Disruption of Bcr-Abl coiled coil oligomerization by design. J Biol Chem. 2011;286:27751–60.

Eide CA, Zabriskie MS, Savage Stevens SL, Antelope O, Vellore NA, Than H, et al. Combining the allosteric inhibitor Asciminib with Ponatinib suppresses emergence of and restores efficacy against highly resistant BCR-ABL1 mutants. Cancer Cell. 2019;36(431–443):431–443.e5.

Frietsch JJ, Kastner C, Grunewald TGP, Schweigel H, Nollau P, Ziermann J, et al. LASP1 is a novel BCR-ABL substrate and a phosphorylation-dependent binding partner of CRKL in chronic myeloid leukemia. Oncotarget. 2014;5:5257–71.

Gambini L, Baggio C, Udompholkul P, Jossart J, Salem AF, Perry JJP, et al. Covalent inhibitors of protein-protein interactions targeting lysine, tyrosine, or histidine residues. J Med Chem. 2019;62:5616–27.

Gehringer M, Laufer SA. Emerging and Re-emerging warheads for targeted covalent inhibitors: Applications in medicinal chemistry and chemical biology. J Med Chem. 2019;62:5673–724.

Gurry T, Stultz CM. Mechanism of amyloid-beta fibril elongation. Biochemistry. 2014;53:6981–91.

He Y, Wertheim JA, Xu L, Miller JP, Karnell FG, Choi JK, et al. The coiled-coil domain and Tyr177 of bcr are required to induce a murine chronic myelogenous leukemia-like disease by bcr/abl. Blood. 2002;99:2957–68.

Huang J, Rauscher S, Nawrocki G, Ran T, Feig M, de Groot BL, et al. CHARMM36m: An improved force field for folded and intrinsically disordered proteins. Nat Methods. 2017;14:71–3.

Hughes TP, Mauro MJ, Cortes JE, Minami H, Rea D, DeAngelo DJ, et al. Asciminib in chronic myeloid leukemia after ABL kinase inhibitor failure. N Engl J Med. 2019;381:2315–26.

Im W, Lee MS, Brooks CL 3rd. Generalized born model with a simple smoothing function. J Comput Chem. 2003;24:1691–702.

Jang H, Arce FT, Ramachandran S, Kagan BL, Lal R, Nussinov R. Disordered amyloidogenic peptides may insert into the membrane and assemble into common cyclic structural motifs. Chem Soc Rev. 2014;43:6750–64.

Jang H, Banerjee A, Chavan T, Gaponenko V, Nussinov R. Flexible-body motions of calmodulin and the farnesylated hypervariable region yield a high-affinity interaction enabling K-Ras4B membrane extraction. J Biol Chem. 2017;292:12544–59.

Jang H, Banerjee A, Marcus K, Makowski L, Mattos C, Gaponenko V, et al. The structural basis of the Farnesylated and methylated KRas4B interaction with Calmodulin. Structure. 2019;27(11):1647–1659.e4.

Jang H, Muratcioglu S, Gursoy A, Keskin O, Nussinov R. Membrane-associated Ras dimers are isoform-specific: K-Ras dimers differ from H-Ras dimers. Biochem J. 2016;473:1719–32.

Jang H, Smith IN, Eng C, Nussinov R. The mechanism of full activation of tumor suppressor PTEN at the phosphoinositide-enriched membrane. iScience. 2021;24:102438.

Kantarjian H, Cortes JE. Complete cytogenetic response, not deep molecular response, is associated with survival in chronic myeloid leukemia. J Clin Oncol. 2014;32:3077–7.

Klauda JB, Venable RM, Freites JA, O'Connor JW, Tobias DJ, Mondragon-Ramirez C, et al. Update of the CHARMM all-atom additive force field for lipids: Validation on six lipid types. J Phys Chem B. 2010;114:7830–43.

Kollman JM, Pandi L, Sawaya MR, Riley M, Doolittle RF. Crystal structure of human fibrinogen. Biochemistry. 2009;48:3877–86.

La Rosee P, Holm-Eriksen S, Konig H, Hartel N, Ernst T, Debatin J, et al. Phospho-CRKL monitoring for the assessment of BCR-ABL activity in imatinib-resistant chronic myeloid leukemia or Ph+ acute lymphoblastic leukemia patients treated with nilotinib. Haematologica. 2008;93:765–9.

Liao TJ, Jang H, Fushman D, Nussinov R. Allosteric KRas4B can modulate SOS1 fast and slow Ras activation cycles. Biophys J. 2018;115:629–41.

Lindström HJG, Friedman R. The effects of combination treatments on drug resistance in chronic myeloid leukaemia: An evaluation of the tyrosine kinase inhibitors axitinib and asciminib. BMC Cancer. 2020;20:397.

Lindström HJG, Friedman R. Rotating between ponatinib and imatinib temporarily increases the efficacy of imatinib as shown in a chronic myeloid leukaemia model. Sci Rep. 2022;12:5164.

Liu F, Hakami RM, Dyas B, Bahta M, Lountos GT, Waugh DS, et al. A rapid oxime linker-based library approach to identification of bivalent inhibitors of the Yersinia pestis protein-tyrosine phosphatase. YopH Bioorg Med Chem Lett. 2010;20:2813–6.

Liu Y, Jang H, Zhang M, Tsai CJ, Maloney R, Nussinov R. The structural basis of BCR-ABL recruitment of GRB2 in chronic myelogenous leukemia. Biophys J. 2022;121:2251–65.

Liu Y, Zhang M, Tsai C, Jang H, Nussinov R. Allosteric regulation of autoinhibition and activation of c-Abl. Comput Struct Biotechnol J. 2022;20:4257–70.

Ludwiczak J, Winski A, Szczepaniak K, Alva V, Dunin-Horkawicz S. DeepCoil-a fast and accurate prediction of coiled-coil domains in protein sequences. Bioinformatics. 2019;35:2790–5.

Lupas AN, Bassler J, Dunin-Horkawicz S. The structure and topology of alpha-helical coiled coils. Subcell Biochem. 2017;82:95–129.

Ma B, Nussinov R. Selective molecular recognition in amyloid growth and transmission and cross-species barriers. J Mol Biol. 2012;421:172–84.

Maloney RC, Zhang M, Jang H, Nussinov R. The mechanism of activation of monomeric B-Raf V600E. Comput Struct Biotechnol J. 2021;19:3349–63.

Manley PW, Barys L, Cowan-Jacob SW. The specificity of asciminib, a potential treatment for chronic myeloid leukemia, as a myristate-pocket binding ABL inhibitor and analysis of its interactions with mutant forms of BCR-ABL1 kinase. Leuk Res. 2020;98:106458.

Mcwhirter JR, Galasso DL, Wang JYJ. A coiled-coil Oligomerization domain of Bcr is essential for the transforming function of Bcr-Abl Oncoproteins. Mol Cell Biol. 1993;13:7587–95.

Mian AA, Schull M, Zhao Z, Oancea C, Hundertmark A, Beissert T, et al. The gatekeeper mutation T315I confers resistance against small molecules by increasing or restoring the ABL-kinase activity accompanied by aberrant transphosphorylation of endogenous BCR, even in loss-of-function mutants of BCR/-ABL. Leukemia. 2009;23:1614–21.

Modi H, Li L, Chu S, Rossi J, Yee JK, Bhatia R. Inhibition of Grb2 expression demonstrates an important role in BCR-ABL-mediated MAPK activation and transformation of primary human hematopoietic cells. Leukemia. 2011;25:305–12.

Mozumdar D, Doerner A, Zhang JY, Rafizadeh DN, Schepartz A. Discrete coiled coil Rotamers form within the EGFRvIII Juxtamembrane domain. Biochemistry. 2020;59:3965–72.

Mughal TI, Radich JP, Deininger MW, Apperley JF, Hughes TP, Harrison CJ, et al. Chronic myeloid leukemia: Reminiscences and dreams. Haematologica. 2016;101:541–58.

Nussinov R, Zhang M, Maloney R, Liu Y, Tsai CJ, Jang H. Allostery: Allosteric cancer drivers and innovative allosteric drugs. J Mol Biol. 2022;434:167569.

Ozdemir ES, Jang H, Gursoy A, Keskin O, Li Z, Sacks DB, et al. Unraveling the molecular mechanism of interactions of the rho GTPases Cdc42 and Rac1 with the scaffolding protein IQGAP2. J Biol Chem. 2018;293:3685–99.

Peiris MN, Meyer AN, Nelson KN, Bisom-Rapp EW, Donoghue DJ. Oncogenic fusion protein BCR-FGFR1 requires the breakpoint cluster region-mediated oligomerization and chaperonin Hsp90 for activation. Haematologica. 2020;105:1262–73.

Peng Y, Huang Z, Zhou F, Wang T, Mou K, Feng W. Effect of HSP90AB1 and CC domain interaction on Bcr-Abl protein cytoplasm localization and function in chronic myeloid leukemia cells. Cell Commun Signal. 2021;19:71.

Phillips JC, Braun R, Wang W, Gumbart J, Tajkhorshid E, Villa E, et al. Scalable molecular dynamics with NAMD. J Comput Chem. 2005;26:1781–802.

Poirier D. Targeting histidine for developing a new generation of covalent enzyme inhibitors. Curr Enzyme Inhib. 2021;17:157–60.

Quach D, Tang G, Anantharajan J, Baburajendran N, Poulsen A, Wee JLK, et al. Strategic design of catalytic lysine-targeting reversible covalent BCR-ABL inhibitors. Angew Chem Int Ed Engl. 2021;60:17131–7.

Reckel S, Gehin C, Tardivon D, Georgeon S, Kükenshöner T, Löhr F, et al. Structural and functional dissection of the DH and PH domains of oncogenic Bcr-Abl tyrosine kinase. Nat Commun. 2017;8:2101.

Ren B, Liu Y, Zhang Y, Zhang M, Sun Y, Liang G, et al. Tanshinones inhibit hIAPP aggregation, disaggregate preformed hIAPP fibrils, and protect cultured cells. J Mater Chem B. 2018;6:56–67.

Ren R. Mechanisms of BCR-ABL in the pathogenesis of chronic myelogenous leukaemia. Nat Rev Cancer. 2005;5:172–83.

Ross TS, Mgbemena VE. Re-evaluating the role of BCR/ABL in chronic myelogenous leukemia. Mol Cell Oncol. 2014;1:e963450.

Schlessinger J. Cell signaling by receptor tyrosine kinases. Cell. 2000;103:211–25.

Schoepfer J, Jahnke W, Berellini G, Buonamici S, Cotesta S, Cowan-Jacob SW, et al. Discovery of Asciminib (ABL001), an allosteric inhibitor of the tyrosine kinase activity of BCR-ABL1. J Med Chem. 2018;61:8120–35.

Shah NP, Sawyers CL. Mechanisms of resistance to STI571 in Philadelphia chromosome-associated leukemias. Oncogene. 2003;22:7389–95.

Smith KM, Yacobi R, Van Etten RA. Autoinhibition of Bcr-Abl through its SH3 domain. Mol Cell. 2003;12:27–37.

Sutanto F, Konstantinidou M, Domling A. Covalent inhibitors: A rational approach to drug discovery. RSC Med Chem. 2020;11:876–84.

Ung PM, DeVita RJ, Schlessinger A. Encounter and react: Computer-guided Design of Covalent Inhibitors. Cell Chem Biol. 2019;26:6–8.

Utterstrom J, Naeimipour S, Selegard R, Aili D. Coiled coil-based therapeutics and drug delivery systems. Adv Drug Deliv Rev. 2021;170:26–43.

Verkhivker GM. Making the invisible visible: Toward structural characterization of allosteric states, interaction networks, and allosteric regulatory mechanisms in protein kinases. Curr Opin Struct Biol. 2021;71:71–8.

Wang EC, Sun HY, Wang JM, Wang Z, Liu H, Zhang JZH, et al. End-point binding free energy calculation with MM/PBSA and MM/GBSA: Strategies and applications in drug design. Chem Rev. 2019;119:9478–508.

Weako J, Jang H, Keskin O, Nussinov R, Gursoy A. The structural basis of Akt PH domain interaction with calmodulin. Biophys J. 2021;120:1994–2008.

Woessner DW, Eiring AM, Bruno BJ, Zabriskie MS, Reynolds KR, Miller GD, et al. A coiled-coil mimetic intercepts BCR-ABL1 dimerization in native and kinase-mutant chronic myeloid leukemia. Leukemia. 2015;29:1668–75.

Wylie AA, Schoepfer J, Jahnke W, Cowan-Jacob SW, Loo A, Furet P, et al. The allosteric inhibitor ABL001 enables dual targeting of BCR-ABL1. Nature. 2017;543:733–7.

Yeung W, Kwon A, Taujale R, Bunn C, Venkat A, Kannan N. Evolution of functional diversity in the Holozoan tyrosine Kinome. Mol Biol Evol. 2021;38:5625–39.

Yin Z, Machius M, Nestler EJ, Rudenko G. Activator protein-1: Redox switch controlling structure and DNA-binding. Nucleic Acids Res. 2017;45:11425–36.

Zhang J, Zhang HY, Wu T, Wang Q, van der Spoel D. Comparison of implicit and explicit solvent models for the calculation of solvation free energy in organic solvents. J Chem Theory Comput. 2017;13:1034–43.

Zhang M, Jang H, Gaponenko V, Nussinov R. Phosphorylated Calmodulin promotes PI3K activation by binding to the SH2 domains. Biophys J. 2017;113:1956–67.

Zhang M, Jang H, Li Z, Sacks DB, Nussinov R. B-Raf autoinhibition in the presence and absence of 14-3-3. Structure. 2021;29(768–777):e762.

Zhang M, Jang H, Nussinov R. The mechanism of PI3Kα activation at the atomic level. Chem Sci. 2019;10:3671–80.

Zhang X, Subrahmanyam R, Wong R, Gross AW, Ren R. The NH(2)-terminal coiled-coil domain and tyrosine 177 play important roles in induction of a myeloproliferative disease in mice by Bcr-Abl. Mol Cell Biol. 2001;21:840–53.

Zhang Y, Zhang M, Liu Y, Zhang D, Tang Y, Ren B, et al. Dual amyloid cross-seeding reveals steric zipper-facilitated fibrillization and pathological links between protein misfolding diseases. J Mater Chem B. 2021;9:3300–16.

Zhao X, Ghaffari S, Lodish H, Malashkevich VN, Kim PS. Structure of the Bcr-Abl oncoprotein oligomerization domain. Nat Struct Biol. 2002;9:117–20.

SUPPORTING INFORMATION

Additional supporting information can be found online in the Supporting Information section at the end of this article.

How to cite this article: Liu Y, Zhang M, Jang H, Nussinov R. Higher-order interactions of Bcr-Abl can broaden chronic myeloid leukemia (CML) drug repertoire. Protein Science. 2023;32(1):e4504. https://doi.org/10.1002/pro.4504